THE JOURNAL OF PHYSICAL CHEMISTRY LETTERS
A JOURNAL OF THE AMERICAN CHEMICAL SOCIETY

pubs.acs.org/JPCL

Letter

Role of Exciton Diffusion and Lifetime in Organic Solar Cells with a Low Energy Offset

Drew B. Riley,* Paul Meredith, Ardalan Armin,* and Oskar J. Sandberg*

Cite This: *J. Phys. Chem. Lett.* 2022, 13, 4402−4409

Read Online

ACCESS | Metrics & More | Article Recommendations

ABSTRACT: Despite general agreement that the generation of free charges in organic solar cells is driven by an energetic offset, power conversion efficiencies have been improved using low-offset blends. In this work, we explore the interconnected roles that exciton diffusion and lifetime play in the charge generation process under various energetic offsets. A detailed balance approach is used to develop an analytic framework for exciton dissociation and free-charge generation accounting for exciton diffusion to and dissociation at the donor−acceptor interface. For low-offset systems, we find the exciton lifetime to be a pivotal component in the charge generation process, as it influences both the exciton and CT state dissociation. These findings suggest that any novel low-offset material combination must have long diffusion lengths with long exciton lifetimes to achieve optimum charge generation yields.

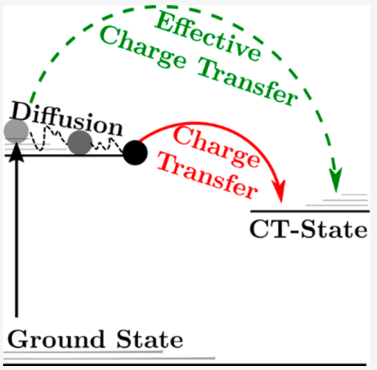

Recently, bulk heterojunction (BHJ) organic solar cells (OSCs) made of blends of electron donating and accepting organic semiconductors have surpassed power conversion efficiencies (PCEs) of 19% with 25% being predicted.[1−4] The recent rise in PCE has been driven by the introduction of narrow-gap nonfullerene acceptors (NFAs), which show enhanced photon absorption of the solar spectrum when used in conjunction with an appropriate and complementary electron donor. This increase in absorption combined with a superior charge generation yield (CGY) observed in state-of-the-art NFA-based BHJs ultimately cumulates in short-circuit currents (J_{SC}) much higher than their fullerene-based predecessors.[5−8] Concurrently, the reduction of energetic offset between donor and acceptor molecules in low-offset NFA BHJs has reduced losses associated with the open-circuit voltage (V_{OC}).[9,10] Specifically, low-offset NFA systems have small energetic differences between the highest occupied molecular orbital (HOMO) levels of the donor and acceptor. As such, the increase in PCE of NFAs, compared to fullerene blends, is ascribable to both the reduction of losses to the V_{OC}, brought about by low HOMO offsets, and the increase in J_{SC}, supported by high CGYs.

The charge generation process in OSCs is typically described stepwise from photon absorption in the active layer to free-charge carrier extraction at the device electrodes.[5,11] Due to the low dielectric constant in organic semiconductors, the primary excitation species upon photon absorption are bound electron−hole pairs, known as excitons, which are localized to either the donor or acceptor phase.[12] To dissociate into free-charge carriers, an exciton must first diffuse to the interface between the donor and acceptor phases of the BHJ, a process that is in competition with the radiative and nonradiative decay of the exciton. After reaching the interface, an exciton in the donor (acceptor) phase can dissociate into a charge-transfer (CT) state by transferring the electron (hole) to the acceptor (donor) phase, referred to as type I (II) charge generation.[13] As the binding energy of CT states is much lower than that of excitons, this intermediate state can dissociate into separated free-charge states (CS states) with relatively high quantum efficiencies.[8,14] While it is widely accepted that increasing the exciton diffusion length enhances the exciton dissociation (via more efficient transfer of excitons to the interface), the influence of exciton diffusion on the charge-transfer efficiency at the interface is not fully understood.

During exciton dissociation, the transfer of an electron (hole) from the donor (acceptor) to the acceptor (donor) phase has been historically understood to be driven by an energetic offset between the lowest unoccupied molecular orbital, or LUMO (HOMO) levels of the two materials.[5,13,15−17] In NFA-based low-offset systems, the driving force to dissociate excitons into CT states at the interface is expected to be small due to the reduced energetic offset. Nonetheless, this has not resulted in a reduction in the CGY,

Received: March 17, 2022
Accepted: May 3, 2022
Published: May 12, 2022

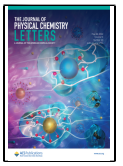

but instead, near unity CGYs have been observed in state-of-the-art low-offset systems.[8] Contributing to the understanding of how NFA BHJs can achieve high CGY in the absence of a significant HOMO offset is the motivation behind this work and a necessary step to further progressing OSC PCEs past 20%.

While a decreasing HOMO offset is expected to reduce energetic losses to the V_{OC}, recent studies have also shown reduced nonradiative voltage losses in low-offset NFA solar cells attributable to an equilibrium between excitons localized to the acceptor phase and CT states.[17,18] On the other hand, it has been suggested that the decreasing driving force for exciton dissociation, brought about through decreasing the HOMO offset, can be compensated for with increasing exciton lifetime.[10,19] Further, it has been shown that photovoltaic parameters such as CGY, J_{SC}, V_{OC}, and PCE are contingent on not only the relative energetics of the donor and acceptor molecules but also the kinetic rate constants between excitons, CT states, and CS states. This includes the interplay between the lifetimes of excitons and CT states as well as the degree of equilibrium between the two states.[3] However, these analyses do not consider the diffusion of excitons to the donor−acceptor interface. Instead, they assume that each exciton generated in the bulk dissociates into a CT state via charge transfer at a rate independent of exciton diffusion.

In this work, the role of exciton diffusion in exciton dissociation and charge generation yield of low-offset organic solar cells is investigated. An expression for the exciton dissociation efficiency and effective dissociation rate constant is derived accounting for the exciton diffusion to and dissociation at the interface. Using this expression, it is clarified under what conditions a system with low driving force for CT state formation can achieve high charge generation yield. It is found that, in low-offset systems, large exciton lifetimes serve a twofold purpose: to increase diffusion to the interface and to reduce the rate of back-transfer of CT states to excitons. Therefore, large diffusion lengths supported by long exciton lifetimes are required for efficient charge generation in low-offset systems.

The process of singlet exciton dissociation is mediated by two steps: (i) diffusion of excitons to the donor−acceptor interface and (ii) charge transfer at the interface with rate constant $k_{CT,0}$. In the case of excitons in the donor (acceptor) phase, $k_{CT,0}$ is the electron (hole) transfer rate constant associated with type I (II) charge generation. In the limit where diffusion to the interface is efficient the exciton dissociation rate is independent of diffusion. In this limit, the efficiency of exciton dissociation (P_S) is given by the charge-transfer efficiency η_{CT} of excitons at the interface, described by the competition between the charge-transfer rate at the interface and the lifetime of the singlet exciton (τ) within the limiting phase as

$$\eta_{CT} = \frac{k_{CT,0}}{1/\tau + k_{CT,0}} \tag{1}$$

In general, away from the diffusion independent limit, the effective rate of exciton dissociation will be given by processes (i) and (ii) occurring in series. To derive an expression for the exciton dissociation efficiency and effective dissociation rate constant, accounting for exciton diffusion to and charge transfer at the interface, we consider a domain of length L, spanning $0 < x < L$, in which excitons are uniformly generated at rate G. Figure 1 shows a schematic state diagram and the relevant rates of diffusion, decay, charge transfer, and CT state-to-exciton back-transfer for a singlet exciton in either the donor or acceptor phase. Under these conditions, the diffusion equation for excitons in the bulk takes the form

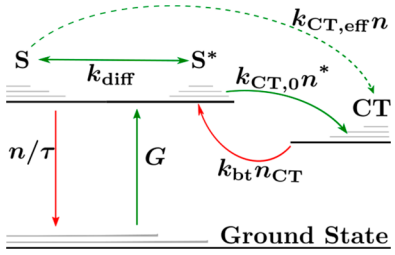

Figure 1. Schematic energy-level diagram showing relevant kinetics and processes occurring for bulk (S) and interfacial (S*) excitons and charge-transfer states (CT). Here, k_{diff} represents the rate constant of diffusion from bulk to interfacial excitonic states, $k_{CT,0}$ is the electron or hole transfer rate constant from interfacial excitons-to-CT states, $k_{bt}n_{CT}$ is the rate of back-transfer from CT states to excitons, τ is the exciton lifetime, G is the rate of exciton generation, and $k_{CT,eff}$ is the effective dissociation rate constant for all excitons.

$$G - \frac{n(x)}{\tau} + D\frac{d^2n(x)}{dx^2} = 0 \tag{2}$$

where $n(x)$ is the exciton density at position x in the domain and D is the diffusion coefficient for the singlet excitons. To account for exciton-to-CT state dissociation and CT state-to-exciton back-transfer, the exciton current leaving the domain at the interfaces can be expressed as

$$-D\frac{dn(x)}{dx}\bigg|_{x=L} = \nu[n(L) - n_{bt}^*] \tag{3}$$

$$-D\frac{dn(x)}{dx}\bigg|_{x=0} = -\nu[n(0) - n_{bt}^*] \tag{4}$$

with ν being the interfacial velocity of charge transfer from one phase to the other and νn_{bt}^* being the exciton current entering the domain via back-transfer from CT states. Here, n_{bt}^* is an effective density that depends on the prevailing density of CT states at the interface but is independent of x. The solution to eqs 2−4 is obtained as

$$n(x) = G\tau - \frac{[G\tau - n_{bt}^*]\cosh\left(\frac{x - L/2}{L_D}\right)}{\cosh\left(\frac{L}{2L_D}\right)\left[1 + \frac{D}{\nu L_D}\tanh\left(\frac{L}{2L_D}\right)\right]} \tag{5}$$

where $L_D = \sqrt{D\tau}$ is the one-dimensional exciton diffusion length.

However, eq 2 does not explicitly contain the exciton-to-CT state charge transfer and CT state-to-exciton back-transfer rates, while eq 5 strongly depends on the position within the domain. Therefore, to obtain a general rate equation that relates excitons in the bulk to excitons at the interface, one can average eq 2 across the domain to obtain

$$G - \frac{n}{\tau} - k_{CT,0}[n^* - n_{bt}^*] = 0 \tag{6}$$

https://doi.org/10.1021/acs.jpclett.2c00791
J. Phys. Chem. Lett. 2022, 13, 4402−4409

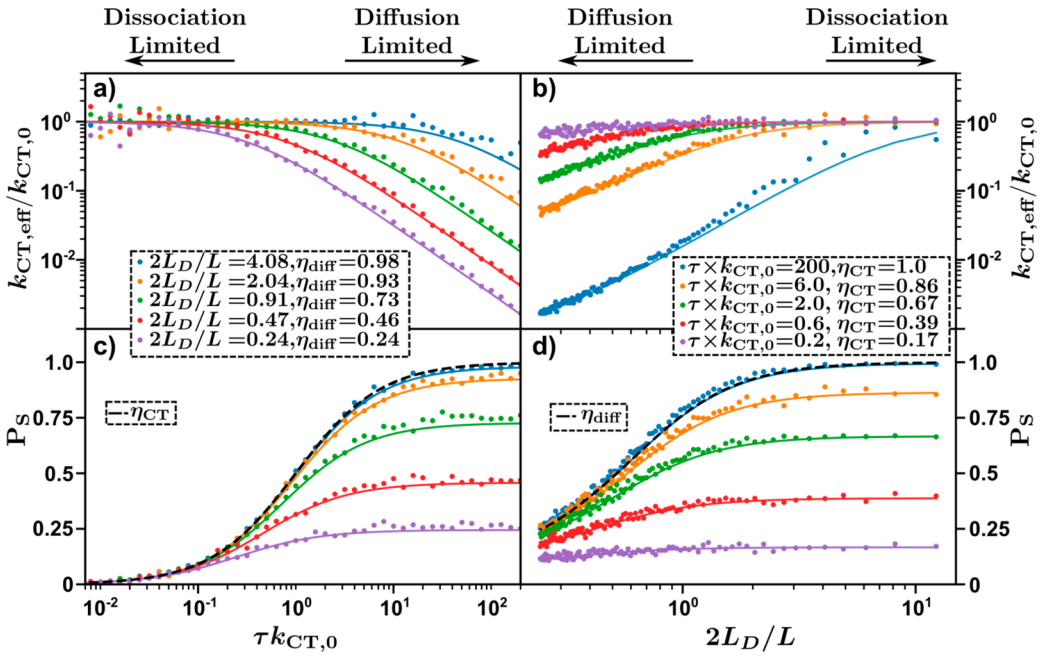

Figure 2. (Top) Normalized effective exciton dissociation rate constant and (Bottom) exciton dissociation efficiency as a function of (left) lifetime-product and (right) the characteristic length ratio. Circles indicate Monte Carlo simulations, solid lines indicate eqs 9 and 11, black dashed lines indicate eqs 1 and 10.

where $n = (1/L)\int_0^L n(x)\mathrm{d}x$ represents the average density of bulk excitons, n^* is the density of excitons at the interfaces, and $k_{CT,0} = 2\nu/L$. Evident in eq 6 is that the CT state-to-exciton back-transfer rate can be equivalently expressed as $k_{CT,0}n_{bt}^*$ or $k_{bt}n_{CT}$ (as shown in Figure 1, where n_{CT} is the density of CT states and k_{bt} is the associated back-transfer rate constant). At thermal equilibrium, the exciton-to-CT state and CT state-to-exciton rates must balance, $k_{bt}n_{CT,eq} = k_{CT,0}n_{eq}^*$, leading to

$$n_{bt}^* = n_{CT}\frac{N_S}{N_{CT}}\exp\left(-\frac{\Delta E_{S/CT}}{k_B T}\right) \tag{7}$$

where k_B is the Boltzmann constant, T is the temperature, E_S (E_{CT}) and N_S (N_{CT}) are the energy and available density of states for the lowest singlet exciton (CT) states, respectively, while $n_{eq}^* = N_S\exp\left(-\frac{E_S}{k_B T}\right)$, $n_{CT,eq} = N_{CT}\exp\left(-\frac{E_{CT}}{k_B T}\right)$, and $\Delta E_{S/CT} = E_S - E_{CT}$ is the energetic offset between the exciton and CT states. Additionally, at thermal equilibrium, the net diffusion current of excitons must vanish such that $n = n^* = n_{bt}^*$, in accordance with detailed balance.

After accounting for this, eq 6 can be equivalently expressed in terms of n as

$$G - \frac{n}{\tau} - k_{CT,eff}[n - n_{bt}^*] = 0 \tag{8}$$

where

$$k_{CT,eff} = \frac{k_{CT,0}}{1 + (\tau \times k_{CT,0})\left[\frac{1-\eta_{diff}}{\eta_{diff}}\right]} \tag{9}$$

is the effective charge-transfer rate constant for excitons generated within the domain, while η_{diff} is the efficiency of exciton diffusion to the interface given by

$$\eta_{diff} = \frac{2L_D}{L}\tanh\left(\frac{L}{2L_D}\right) \tag{10}$$

Finally, the overall exciton dissociation efficiency, defined as the number of dissociated excitons relative to the total number of generated excitons can be found as

$$P_S = \frac{k_{CT,eff}}{\frac{1}{\tau} + k_{CT,eff}} = \left[\frac{1}{\eta_{diff}} + \frac{1}{\eta_{CT}} - 1\right]^{-1} \tag{11}$$

where eqs 1 and 9 were used in the last step. Note that P_S is not given by the simple product of the diffusion and dissociation efficiencies, indicating that processes (i) and (ii) are not independent.

To substantiate eqs 9 and 11, a 1D Monte Carlo hopping model was implemented to simulate the exciton kinetics including diffusion, decay, and interfacial charge transfer. Monte Carlo simulations were used, as they have been shown to accurately account for exciton dynamics within organic semiconductors and BHJs.[20−26] Furthermore, the use of Monte Carlo simulations allows for the calculation of the exciton dissociation efficiency and effective dissociation rate constant under conditions where the domain size, dissociation rate constant at the interface, exciton lifetime, and exciton diffusion coefficient are known precisely. The simulated dissociation efficiency and effective dissociation rate constant can then be compared to eqs 9 and 11. The details of the simulation are outlined in the Methods section. The exciton dissociation efficiency was calculated as the ratio of excitons exiting the domain at the interfaces to the total number of excitons generated in the simulation, from which the effective dissociation rate constant can be calculated through eq 11. In this formalism, the characteristic length ratio (defined as $2L_D/L$) and the lifetime-product (defined as $\tau \times k_{CT,0}$) can be controlled by specifying the domain size and interfacial charge-transfer rate constant, respectively, while leaving the exciton

https://doi.org/10.1021/acs.jpclett.2c00791
J. Phys. Chem. Lett. 2022, 13, 4402−4409

lifetime and diffusion coefficient unaffected. It is important to note that, in general, these two metrics are not independent, as increases in the exciton lifetime will affect both the lifetime-product and the diffusion length. The effect on these metrics of changing the diffusion constant and lifetime are discussed throughout the remainder of this contribution. In these simulations, the exciton lifetime was 300 ps, while the diffusion coefficient was of 5×10^{-3} cm^2/s, leading to L_D = 12 nm.

Figure 2 shows the normalized effective dissociation rate constant and exciton dissociation efficiency as a function of the lifetime-product for selected diffusion efficiencies, determined by the characteristic length ratio through eq 10 (Figure 2a,c), and the characteristic length ratio for various charge-transfer efficiencies, determined by the lifetime-product through eq 1 (Figure 2b,d). The circles indicate values from the Monte Carlo simulations, while the colored lines indicate eqs 9 and 11 plotted with the associated values of τ, $k_{CT,0}$, L, and D. The analytic solution provided by eqs 9 and 11 reproduces the simulated P_S and $k_{CT,eff}$ over the range of parameters used. As noted above, exciton dissociation can be limited by two distinct processes: diffusion to the interface and dissociation at the interface. As will be shown below, both these processes must be efficient for excitons generated in the domain to be dissociated efficiently.

Under conditions when either $\tau \times k_{CT,0}$ is small or $2L_D/L$ is large, corresponding to $\eta_{CT} \ll \eta_{diff}$ or $\eta_{diff} \to 1$, respectively, the overall dissociation rate of excitons is dissociation limited. As indicated on the left-hand side of Figure 2a and right-hand side of Figure 2b, this limit is characterized by $k_{CT,eff} \to k_{CT,0}$. Under these conditions, the dissociation at the interface is the rate-limiting process, and according to eq 11, $P_S = \eta_{CT}$ (indicated by the black dashed line in Figure 2c). In the dissociation limited regime, P_S is strongly dependent on lifetime-product, asymptotically approaching $P_S = 0$ with decreasing lifetime-product. Conversely, under conditions when $\tau \times k_{CT,0}$ is large (right-hand side of Figure 2a) or $2L_D/L$ is small (left-hand side of Figure 2b), corresponding to $\eta_{CT} \to 1$ or $\eta_{diff} \ll \eta_{CT}$, respectively, the exciton dissociation is diffusion limited. In this limit, diffusion to the interface is the rate-limiting process, resulting in $k_{CT,eff}/k_{CT,0} \ll 1$ and $P_S = \eta_{diff}$ (indicated by the black dashed line in Figure 2d). In this limit, P_S is dependent only on the characteristic length ratio and approaches $P_S = 0$ for a diminishing characteristic length ratio, as excitons are unable to diffuse to the interface. Finally, under conditions when both $\tau \times k_{CT,0}$ and $2L_D/L$ exceed unity, shown on the right-hand sides of Figure 2c as $\eta_{diff} \to 1$ and Figure 2d as $\eta_{CT} \to 1$, eventually $P_S \to 1$.

This analysis is summarized in Figure 3, which shows the simulated P_S (Figure 3a) and $k_{CT,eff}$ (Figure 3b) as a function of the lifetime-product and the characteristic length ratio. Indicated on Figure 3 is the diffusion and dissociation limits. For a dissociation limited system, changes to the characteristic length ratio will not significantly affect $k_{CT,eff}$ or P_S. This can be recognized by moving vertically in Figure 3 in the dissociation limited regime. Similarly, for a diffusion limited system, changes to the lifetime-product will not significantly alter $k_{CT,eff}$ or P_S. This can be recognized by moving horizontally in Figure 3 in the diffusion limited regime.

These observations highlight the primary thesis of this work: to efficiently dissociate excitons into CT states, the phase limiting charge generation must simultaneously have efficient diffusion to and dissociation at the interface, enabled by high lifetime-products and characteristic length ratios. The former

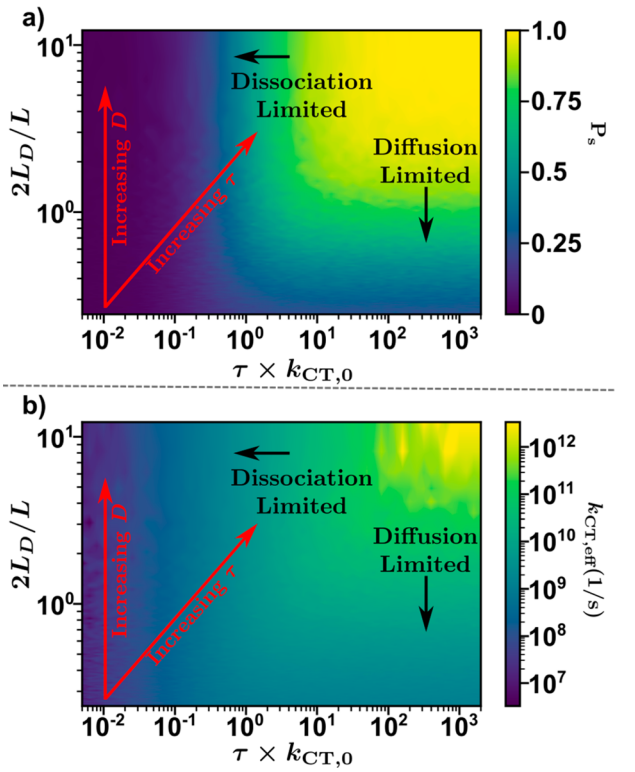

Figure 3. (a) Exciton dissociation efficiency and (b) effective exciton dissociation rate constant as a function of characteristic length ratio and lifetime-product. Red lines indicate the direction a system will move for an increasing exciton diffusion constant and lifetime.

can be increased by increasing the exciton lifetime or increasing the dissociation rate constant at the interface. The latter can be increased by increasing the diffusion length, via increases in exciton lifetime or diffusion constant, or by decreasing the domain size.[27,28] Therefore, the exciton lifetime plays a crucial role in determining the exciton dissociation efficiency, as increases in exciton lifetime increase both the characteristic length ratio and lifetime-product. This observation agrees with previous experimental studies by other researchers.[10] Despite this, the diffusion constant plays an equally important role in determining the characteristic length ratio and therefore is important in determining the diffusion efficiency, the dissociation efficiency, and effective dissociation rate constant. This is highlighted by the red lines in Figure 3. Increases in diffusion constant lead to increases in the characteristic length ratio, manifesting in a vertical transition in Figure 3, while increases in the exciton lifetime increase both the characteristic length ratio as well as the lifetime-product, signified by the sloped red lines in Figure 3.

To explore the effects that exciton diffusion has on the device performance of organic solar cells, the charge generation yield (P_{CGY}) was calculated. Here, P_{CGY} is defined as the ratio of generated CS states to the total number of generated excitons. To calculate P_{CGY}, the kinetic interplay between excitons, CT states, and CS states is considered,[3] as described in detail in the Methods section. After accounting for the generation, recombination, reformation, and dissociation of CT states and excitons, summarized in Figure 4a, we find $P_{CGY} = P_S P_{CT}$, where $P_{CT} = k_d/(k_d + k_f + k'_{bt})$ denotes the CT state-to-CS state dissociation efficiency. Further, k_d is the CT state dissociation rate constant, k_f is the CT state recombination rate

https://doi.org/10.1021/acs.jpclett.2c00791
J. Phys. Chem. Lett. 2022, 13, 4402−4409

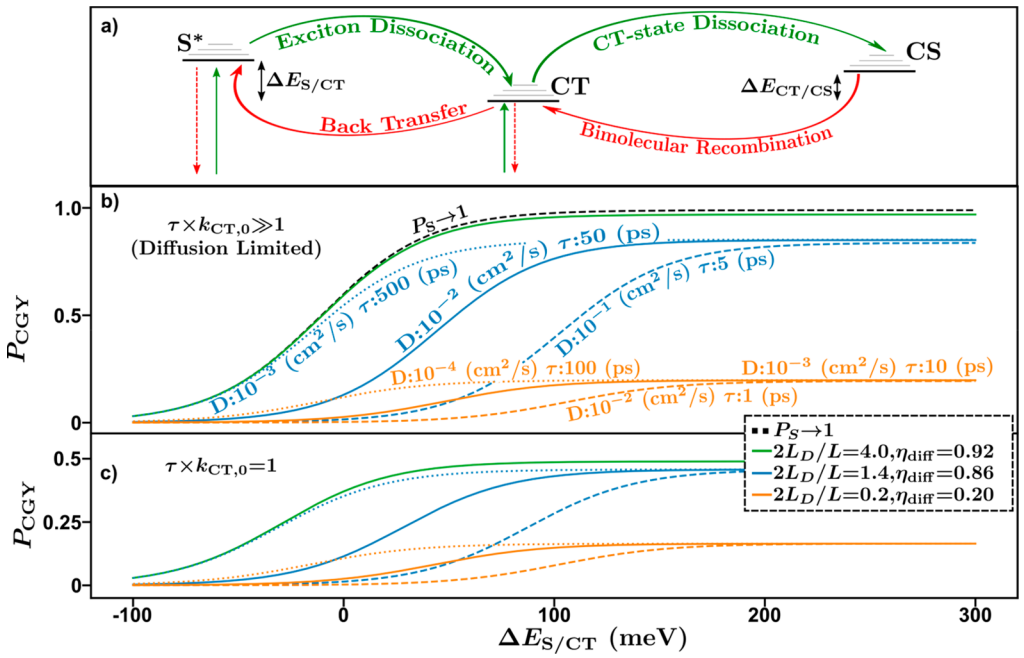

Figure 4. (a) Schematic energy-level diagram summarizing the work of Sandberg et al.[3] Labeled are interfacial excitonic states (S*), charge-transfer states (CT), and charge separated states (CS), as well as the varying pathways between them and to the ground state (vertical arrows). Charge generation yield as a function of exciton-to-CT state offset for a system with (a) large and (b) unity lifetime-products. The black dashed line indicates the conclusion of Sandberg et al.[3] Colors of lines indicate the characteristic length ratios. Moving from dotted to solid to dashed lines indicates increasing exciton diffusion constant and decreasing exciton lifetime.

constant, and $k'_{bt} = (1 - P_S)k_{bt,eff}$. Finally, $k_{bt,eff}$ is the effective CT-to-exciton back-transfer rate constant related to $k_{CT,eff}$ via $k_{bt,eff} = (n^*_{bt}/n_{CT})k_{CT,eff}$; hence,

$$k'_{bt} = \frac{P_S N_S}{\tau N_{CT}} \exp\left[-\frac{\Delta E_{S/CT}}{K_B T}\right] \tag{12}$$

in accordance with eqs 7 and 11. Consequentially, CT states generated directly from the ground state or via interfacial charge transfer may form excitons via this back-transfer mechanism and reform CT states many times over.

The idealized case for P_{CGY} with efficient diffusion, corresponding to $\eta_{diff} = 1$, is shown for a high interfacial charge-transfer rate in the dashed black line in Figure 4b. The calculated P_{CGY} as a function of the exciton-to-CT state energetic offset ($\Delta E_{S/CT}$) is summarized in Figure 4b,c for the lifetime-products $\tau \times k_{CT,0} \gg 1$ and $\tau \times k_{CT,0} = 1$, respectively, assuming a domain size of 10 nm. In the case of a high lifetime-product (equivalent to the diffusion limited regime), eq 11 simplifies to $P_S = \eta_{diff}$. Therefore, as the characteristic length ratio is increased, exciton dissociation is increased. This results in an increase in P_{CGY} with an increasing characteristic length ratio independent of $\Delta E_{S/CT}$, generally seen by comparing the different colored lines in Figure 4b.

Interestingly, in the high-offset limit ($\Delta E_{S/CT} > 200$ meV) P_{CGY} is dependent on the characteristic length ratio yet agnostic to the individual values of τ and D. This effect can be observed by comparing lines of the same color in the high-offset region of Figure 4b,c. On the other hand, for low-offset systems ($\Delta E_{S/CT} < 200$ meV), the CT state-to-exciton back-transfer plays a more central role in determining the P_{CGY}. In this case, the rate of CT states undergoing back-transfer to form excitons is much higher, which in turn increases the likelihood that excitons will reform and decay. Therefore, it is expected that a higher exciton lifetime will decrease the number of CT states that recombine to the ground state via an excitonic state by the back-transfer mechanism and, in turn, increase the P_{CGY}. This effect is evident in comparing the dotted (longest τ), solid (middle τ), and dashed (shortest τ) lines of the same color (equivalent L_D) in the low-offset region of Figure 4b. In this region, P_{CGY} for identical characteristic length ratios is increased with increasing exciton lifetime due to decreasing CT state-to-exciton back-transfer.

This highlights the secondary thesis of this work; in low-offset systems, high exciton lifetimes increase not only the exciton dissociation through increased diffusion lengths, as shown by other researchers in previous experimental studies,[10,19] but additionally increase the CGY by ultimately decreasing the rate of CT state-to-exciton back-transfer. The inverse relationship between the CT state-to-exciton back-transfer rate and the exciton lifetime is expressed explicitly in eq 12. Interestingly, NFAs show a significant increase in diffusion length compared to their fullerene predecessors, which would help to explain the improvements in CGY. However, it has been shown that this increase is due primarily to increases in diffusion constants.[26,29−31] The results from Figure 4b suggest that CGY in NFA blends could be dramatically increased by focusing on blends containing low-offset acceptors that have long diffusion lengths supported by increased exciton lifetimes. Systems of this type would increase the diffusion of excitons to the interface while simultaneously reducing CT state-to-exciton back-transfer losses.

Figure 4c shows the equivalent analysis for systems with the same characteristic length ratios but with a lifetime-product of unity, corresponding to $\eta_{CT} = 0.5$. Under these conditions, the exciton dissociation efficiency is expressed as $P_S = \eta_{diff}/(1 + \eta_{diff})$, resulting in a maximal efficiency of 0.5. In general, decreases in the exciton lifetime will decrease the exciton

https://doi.org/10.1021/acs.jpclett.2c00791
J. Phys. Chem. Lett. 2022, 13, 4402−4409

dissociation efficiency via decreases to both the characteristic length ratio, as described above, and the lifetime-product. This additional effect is equivalent to excitons reaching the interface but being unable to dissociate into CT states, effectively "reflecting" off the interface. Therefore, even in the case of high characteristic length ratios and high energetic offsets, such as that shown by the green curve in Figure 4c, the P_{CGY} is reduced via reductions to the effective exciton dissociation rate constant.

In conclusion, the role that exciton diffusion plays in exciton dissociation in BHJ OSCs was investigated and analytic expressions for the exciton dissociation efficiency and the effective dissociation rate constant were derived. This analysis revealed that the exciton dissociation efficiency is determined by the efficiency of exciton diffusion to the interface (determined by the characteristic length ratio, $2L_D/L$) and the charge-transfer efficiency at the interface (determined by the lifetime-product, $\tau \times k_{CT,0}$). The expression for exciton dissociation efficiency was used to calculate the theoretical charge generation yield in BHJ OSCs. For high-offset systems, it was found that the charge generation yield is governed by the characteristic length ratio and that the individual values of exciton lifetime and diffusion coefficient were inconsequential. However, in low-offset systems, the exciton lifetime influences not only the characteristic length ratio but also the rate of back-transfer from CT states to excitons. Therefore, the exciton lifetime plays a more critical role than the diffusion constant in determining the charge generation yield in low-offset systems. This work provides a framework for discussing the effect exciton diffusion has on both the exciton dissociation and the charge generation yield in organic solar cells, from which other photovoltaic parameters can be calculated. Our analysis suggests that future materials developed for low-offset organic bulk heterojunction solar cells must exhibit high diffusion lengths to support efficient exciton dissociation and that these diffusion lengths must include long exciton lifetimes to support efficient CT state dissociation.

METHODS

Monte Carlo Simulations. With the aim of modeling the exciton dynamics within an organic semiconductor, a 1D Monte Carlo hopping model was invoked.[25] First, a domain of size L with lattice spacing (dx) is created, and the lattice is randomly populated with an exciton and allowed to evolve in time with a temporal time step size (dt). The diffusion constant in the film is determined as $D = dx^2/2dt$. The lattice spacing, temporal step size, and exciton lifetime (τ) were 1 nm, 1 ps, and 300 ps respectively, corresponding to a diffusion coefficient of 5×10^{-3} cm^2/s and diffusion length of 12 nm ($L_D = \sqrt{D\tau}$). To explore the dependence on the characteristic length ratio ($2L_D/L$), the domain size was varied from 2 to 100 nm. To investigate the effect of the lifetime-product ($\tau \times k_{CT,0}$), the interfacial velocity of charge transfer was varied. This was accomplished by considering the rate of dissociation at the interface (k_{int}) to be related to the interfacial velocity as $\nu = k_{int}dx/2$, and therefore, $k_{int} = k_{CT,0}(L/dx)$. The exciton dissociation efficiency was calculated as the ratio of excitons exiting the domain at the interfaces to the total number of excitons generated in the simulation, from which the effective dissociation rate can be calculated through eq 11.

Charge Generation Yield Calculations. In accordance with eq 6 in the main text, accounting for diffusion to and dissociation at the interface, under steady-state illumination, the kinetics of excitons and CT states is governed by the rate equations

$$G - k_s n - k_{CT,0} n^* + k_{bt} n_{CT} = 0 \tag{A1}$$

$$G_{CT} + k_{CT,0} n^* - k_{bt} n_{CT} - k_f n_{CT} - k_d n_{CT} + \beta_0 n_{CS}^2 = 0 \tag{A2}$$

where G (G_{CT}) is the generation of excitons (CT states) from the ground state, n is the spatially averaged density of excitons in the domain, n^* is density of excitons at the interface, k_s is the decay rate of excitons ($k_s = 1/\tau$), $k_{CT,0}$ is the dissociation rate constant of interfacial excitons, k_{bt} is the back-transfer rate constant, n_{CT} is the density of CT states, k_f is the decay rate constant of CT states, k_d is the rate constant for the dissociation of CT states into charge separated (CS) states, n_{CS} is the density of charge separated states, and β_0 is the bimolecular recombination rate constant of CS states to CT states. However, as established in Section 2 of the main text, after accounting for exciton diffusion to the interface, the net exciton-to-CT rate can be equivalently expressed as $k_{CT,0}n^* - k_{bt}n_{CT} = k_{CT,eff}n - k_{bt,eff}n_{CT}$, where $k_{bt,eff} = k_{bt}k_{CT,eff}/k_{CT,0}$ and $k_{CT,eff}$ is the effective dissociation rate constant described by eq 9. Hence, eqs A1 and A2 can be rewritten as

$$G - k_s n - k_{CT,eff} n + k_{bt,eff} n_{CT} = 0 \tag{A3}$$

$$G_{CT} + k_{CT,eff} n - k_{bt,eff} n_{CT} - k_f n_{CT} - k_d n_{CT} + \beta_0 n_{CS}^2 = 0 \tag{A4}$$

Then, based on eqs A3 and A4, and following the formalism of Sandberg et al.,[3] the CT state-to-CS state dissociation efficiency can be calculated from the decay rate of CT states, the CT state-to-CS state dissociation, and back-transfer rate from CT states to excitons as $P_{CT} = k_d/(k'_{bt} + k_d + k_f)$, where $k'_{bt} = (1 - P_S)k_{bt,eff}$ is the ultimate (effective) back-transfer rate constant. Using a detailed balance approach, the back-transfer rate constant can be calculated as

$$k'_{bt} = \frac{P_S k_s N_S}{N_{CT}} \exp\left[-\frac{\Delta E_{S/CT}}{K_B T}\right] \tag{A5}$$

where N_S and N_{CT} are the density of states for singlet excitons and CT states, respectively, and $\Delta E_{S/CT}$ is the energetic difference between the exciton and CT state. The rate constant for CT state-to-CS state dissociation can be calculated as

$$k_d = \frac{\beta_0 N_{CS}^2}{N_{CT}} \exp\left[-\frac{\Delta E_{CT/CS}}{K_B T}\right] \tag{A6}$$

where N_{CS} is the density of states for CS states and $\Delta E_{CT/CS}$ is the effective CT state binding energy. The charge generation yield can then be expressed as the product of the exciton dissociation efficiency and the CT state dissociation efficiency.

$$P_{CGY} = P_S \times P_{CT} = \frac{P_S}{1 + \frac{k_f N_{CT}}{\beta_0 N_{CS}^2} \exp\left[\frac{\Delta E_{CS/CT}}{K_B T}\right]\left[1 + \frac{P_S k_s N_S}{k_f N_{CT}} \exp\left[\frac{\Delta E_{S/CT}}{K_B T}\right]\right]} \tag{A7}$$

The calculations in Figure 4b,c were performed by evaluating P_S from eq 11 and using the result to calculate P_{CGY} from eq A7. In this work, the default values for the parameters were taken from Sandberg et al. as $k_f = 10^{10}$ s^{-1}, $\beta_0 = 5 \times 10^{-10}$ cm^3 s^{-1}, $N_{CT} = 10^{18}$ cm^{-3}, $N_S = N_{CS} = 3 \times 10^{20}$

https://doi.org/10.1021/acs.jpclett.2c00791
J. Phys. Chem. Lett. 2022, 13, 4402−4409

cm^{-3}, T = 300 K, and $\Delta E_{CS/CT}$ = 100 meV. Meanwhile, the values for k_S and P_S are determined by the choice of τ and D, as shown for each calculation in Figure 4b.

AUTHOR INFORMATION

Corresponding Authors

Drew B. Riley − *Sustainable Advanced Materials Programme (Sêr SAM), Department of Physics, Swansea University, Swansea SA2 8PP, United Kingdom;* orcid.org/0000-0001-6688-0694; Email: 1915821@swansea.ac.uk

Ardalan Armin − *Sustainable Advanced Materials Programme (Sêr SAM), Department of Physics, Swansea University, Swansea SA2 8PP, United Kingdom;* orcid.org/0000-0002-6129-5354; Email: ardalan.armin@swansea.ac.uk

Oskar J. Sandberg − *Sustainable Advanced Materials Programme (Sêr SAM), Department of Physics, Swansea University, Swansea SA2 8PP, United Kingdom;* orcid.org/0000-0003-3778-8746; Email: o.j.sandberg@swansea.ac.uk

Author

Paul Meredith − *Sustainable Advanced Materials Programme (Sêr SAM), Department of Physics, Swansea University, Swansea SA2 8PP, United Kingdom*

Complete contact information is available at: https://pubs.acs.org/10.1021/acs.jpclett.2c00791

Notes

The authors declare no competing financial interest.

ACKNOWLEDGMENTS

This work was supported by the Welsh Government's Sêr Cymru II Program through the European Regional Development Fund, Welsh European Funding Office, and the Swansea University strategic initiative in Sustainable Advanced Materials. A.A. is a Sêr Cymru II Rising Star Fellow, and P.M. is a Sêr Cymru II National Research Chair. This work was also funded by UKRI through the EPSRC Program Grant EP/T028511/1 Application Targeted Integrated Photovoltaics. D.B.R. acknowledges the support of the Natural Sciences and Engineering Research Council of Canada (NSERC), [PGSD3-545694-2020].

REFERENCES

(1) Liu, Q.; Jiang, Y.; Jin, K.; Qin, J.; Xu, J.; Li, W.; Xiong, J.; Liu, J.; Xiao, Z.; Sun, K.; et al. 18% Efficiency organic solar cells. *Sci. Bull.* **2020**, *65*, 272−275.

(2) Azzouzi, M.; Yan, J.; Kirchartz, T.; Liu, K.; Wang, J.; Wu, H.; Nelson, J. Nonradiative energy losses in bulk-heterojunction organic photovoltaics. *Phys. Rev. X* **2018**, *8*, 031055.

(3) Sandberg, O. J.; Armin, A. Energetics and Kinetics Requirements for Organic Solar Cells to Break the 20% Power Conversion Efficiency Barrier. *J. Phys. Chem. C* **2021**, *125*, 15590−15598.

(4) Cui, Y.; Xu, Y.; Yao, H.; Bi, P.; Hong, L.; Zhang, J.; Zu, Y.; Zhang, T.; Qin, J.; Ren, J.; et al. Single-Junction Organic Photovoltaic Cell with 19% Efficiency. *Adv. Mater.* **2021**, *33*, 2102420.

(5) Armin, A.; Li, W.; Sandberg, O. J.; Xiao, Z.; Ding, L.; Nelson, J.; Neher, D.; Vandewal, K.; Shoaee, S.; Wang, T.; et al. A History and Perspective of Non-Fullerene Electron Acceptors for Organic Solar Cells. *Adv. Energy Mater.* **2021**, *11*, 2003570.

(6) Xiao, Z.; Jia, X.; Li, D.; Wang, S.; Geng, X.; Liu, F.; Chen, J.; Yang, S.; Russell, T. P.; Ding, L. 26 mA cm- 2 Jsc from organic solar cells with a low-bandgap nonfullerene acceptor. *Sci. Bull.* **2017**, *62*, 1494−1496.

(7) Wang, X.; Chen, H.; Yuan, J.; Wei, Q.; Li, J.; Jiang, L.; Huang, J.; Li, Y.; Li, Y.; Zou, Y. Precise fluorination of polymeric donors towards efficient non-fullerene organic solar cells with enhanced open circuit voltage, short circuit current and fill factor. *J. Mater. Chem. A* **2021**, *9*, 14752−14757.

(8) Li, W.; Zeiske, S.; Sandberg, O. J.; Riley, D. B.; Meredith, P.; Armin, A. Organic solar cells with near-unity charge generation yield. *Energy Environ. Sci.* **2021**, *14*, 6484−6493.

(9) Eisner, F. D.; Azzouzi, M.; Fei, Z.; Hou, X.; Anthopoulos, T. D.; Dennis, T. J. S.; Heeney, M.; Nelson, J. Hybridization of local exciton and charge-transfer states reduces nonradiative voltage losses in organic solar cells. *J. Am. Chem. Soc.* **2019**, *141*, 6362−6374.

(10) Classen, A.; Chochos, C. L.; Lüer, L.; Gregoriou, V. G.; Wortmann, J.; Osvet, A.; Forberich, K.; McCulloch, I.; Heumüller, T.; Brabec, C. J. The role of exciton lifetime for charge generation in organic solar cells at negligible energy-level offsets. *Nat. Energy* **2020**, *5*, 711−719.

(11) Clarke, T. M.; Durrant, J. R. Charge photogeneration in organic solar cells. *Chem. Rev.* **2010**, *110*, 6736−6767.

(12) Fu, Z.; Zhang, X.; Zhang, H.; Li, Y.; Zhou, H.; Zhang, Y. On the understandings of dielectric constant and its impacts on the photovoltaic efficiency in organic solar cells. *Chin. J. Chem.* **2021**, *39*, 381−390.

(13) Stoltzfus, D. M.; Donaghey, J. E.; Armin, A.; Shaw, P. E.; Burn, P. L.; Meredith, P. Charge generation pathways in organic solar cells: assessing the contribution from the electron acceptor. *Chem. Rev.* **2016**, *116*, 12920−12955.

(14) Perdigón-Toro, L.; Zhang, H.; Markina, A.; Yuan, J.; Hosseini, S. M.; Wolff, C. M.; Zuo, G.; Stolterfoht, M.; Zou, Y.; Gao, F.; et al. Barrierless free charge generation in the high-performance PM6: Y6 bulk heterojunction non-fullerene solar cell. *Adv. Mater.* **2020**, *32*, 1906763.

(15) Armin, A.; Kassal, I.; Shaw, P. E.; Hambsch, M.; Stolterfoht, M.; Lyons, D. M.; Li, J.; Shi, Z.; Burn, P. L.; Meredith, P. Spectral dependence of the internal quantum efficiency of organic solar cells: Effect of charge generation pathways. *J. Am. Chem. Soc.* **2014**, *136*, 11465−11472.

(16) Deibel, C.; Dyakonov, V. Polymer−fullerene bulk heterojunction solar cells. *Rep. Prog. Phys.* **2010**, *73*, 096401.

(17) Hinrichsen, T. F.; Chan, C. C. S.; Ma, C.; Paleček, D.; Gillett, A.; Chen, S.; Zou, X.; Zhang, G.; Yip, H.-L.; Wong, K. S.; et al. Long-lived and disorder-free charge transfer states enable endothermic charge separation in efficient non-fullerene organic solar cells. *Nat. Commun.* **2020**, *11*, 5617.

(18) Perdigón-Toro, L.; Phuong, L. Q.; Zeiske, S.; Vandewal, K.; Armin, A.; Shoaee, S.; Neher, D. Excitons dominate the emission from PM6: Y6 solar cells, but this does not help the open-circuit voltage of the device. *ACS Energy Lett.* **2021**, *6*, 557−564.

(19) Guo, Q.; Liu, Y.; Liu, M.; Zhang, H.; Qian, X.; Yang, J.; Wang, J.; Xue, W.; Zhao, Q.; Xu, X.; et al. Enhancing the performance of organic solar cells by prolonging the lifetime of photogenerated excitons. *Adv. Mater.* **2020**, *32*, 2003164.

(20) Bottenfield, C. G.; Wei, F.; Park, H. J.; Guo, L. J.; Li, G. Investigation of Printing-Based Graded Bulk-Heterojunction Organic Solar Cells. *Energy Technol-Ger* **2015**, *3*, 414−422.

(21) Bässler, H. Charge transport in disordered organic photoconductors. A Monte Carlo simulation study. *Phys. Status. Solidi. B* **1993**, *175*, 15−56.

(22) Kimber, R. G. E.; Wright, E. N.; O'Kane, S. E. J.; Walker, A. B.; Blakesley, J. C. Mesoscopic kinetic Monte Carlo modeling of organic photovoltaic device characteristics. *Phys. Rev. B* **2012**, *86*, 235206.

(23) Watkins, P. K.; Walker, A. B.; Verschoor, G. L. B. Dynamical Monte Carlo modelling of organic solar cells: The dependence of internal quantum efficiency on morphology. *Nano Lett.* **2005**, *5*, 1814−1818.

(24) Zarrabi, N.; Yazmaciyan, A.; Meredith, P.; Kassal, I.; Armin, A. Anomalous exciton quenching in organic semiconductors in the low-yield limit. *J. Phys. Chem. Lett.* **2018**, *9*, 6144−6148.

(25) Kaiser, W.; Popp, J.; Rinderle, M.; Albes, T.; Gagliardi, A. Generalized kinetic Monte Carlo framework for organic electronics. *Algorithms* **2018**, *11*, 37.
(26) Riley, D. B.; Sandberg, O. J.; Li, W.; Meredith, P.; Armin, A. Quasi-Steady-State Measurement of Exciton Diffusion Lengths in Organic Semiconductors. *Phys. Rev. Appl.* **2022**, *17*, 024076.
(27) Lou, S. J.; Szarko, J. M.; Xu, T.; Yu, L.; Marks, T. J.; Chen, L. X. Effects of additives on the morphology of solution phase aggregates formed by active layer components of high-efficiency organic solar cells. *J. Am. Chem. Soc.* **2011**, *133*, 20661−20663.
(28) Neupane, U.; Bahrami, B.; Biesecker, M.; Baroughi, M. F.; Qiao, Q. Kinetic Monte Carlo modeling on organic solar cells: Domain size, donor-acceptor ratio and thickness. *Nano Energy* **2017**, *35*, 128−137.
(29) Cha, H.; Wheeler, S.; Holliday, S.; Dimitrov, S. D.; Wadsworth, A.; Lee, H. H.; Baran, D.; McCulloch, I.; Durrant, J. R. Influence of blend morphology and energetics on charge separation and recombination dynamics in organic solar cells incorporating a nonfullerene acceptor. *Adv. Funct. Mater.* **2018**, *28*, 1704389.
(30) Chandrabose, S.; Chen, K.; Barker, A. J.; Sutton, J. J.; Prasad, S. K. K.; Zhu, J.; Zhou, J.; Gordon, K. C.; Xie, Z.; Zhan, X.; et al. High exciton diffusion coefficients in fused ring electron acceptor films. *J. Am. Chem. Soc.* **2019**, *141*, 6922−6929.
(31) Firdaus, Y.; Le Corre, V. M.; Karuthedath, S.; Liu, W.; Markina, A.; Huang, W.; Chattopadhyay, S.; Nahid, M. M.; Nugraha, M. I.; Lin, Y.; et al. Long-range exciton diffusion in molecular non-fullerene acceptors. *Nat. Commun.* **2020**, *11*, 5220.

https://doi.org/10.1021/acs.jpclett.2c00791
J. Phys. Chem. Lett. 2022, 13, 4402−4409